PROBING DYNAMIC EVOLUTION IN INTERMEDIATE ENERGY COLLISIONS*

J.B. Natowitz, J. Cibor[†], A. Bonasera[‡], K. Hagel, R. Wada
M. Murray, T. Keutgen, M. Lunardon[§], N. Marie[¶], R. Alfaro[‖]
W. Shen[††], Z. Majka[‡‡] and P. Staszel[§§]

Cyclotron Institute, Texas A&M University, College Station
Texas 77843-3366, USA

Molecular dynamics calculations which are employed to model light particle emission in nuclear collisions at intermediate energies suggest that coalescence model analyses may be used to probe the time evolution of these systems and to provide information on the degree of thermal, chemical and isospin equilibrium achieved at particular stages of this evolution. This talk discusses the application of coalescence model analyses to explore light particle emission in reactions between 47A MeV projectiles and medium mass targets. The results provide evidence for increasing expansion of the hot composite nuclei as the projectile mass increases. Densities and temperatures of the freeze-out configurations in multi-fragmenting systems are derived.

PACS numbers: 25.70.–z, 25.70.Pq

1. Introduction

When a central collision of two heavy nuclei leads to multifragmentation of an expanded and equilibrated nucleus the thermal shock and compression which result can cause the nucleus to expand to low density, cluster and disassemble. In order to understand the properties of highly excited nuclei produced in heavy ion collisions it is very desirable to extract, directly from the experimental data if possible, information on the dynamical and thermodynamical evolution of the interaction region and the extent to which equilibration of various degrees of freedom, thermal, chemical, isospin, *etc.*, is realized.

THERMAL SHOCK   FREEZEOUT   SECONDARY
COMPRESSION   EMISSION

EXPANSION   SEPARATION
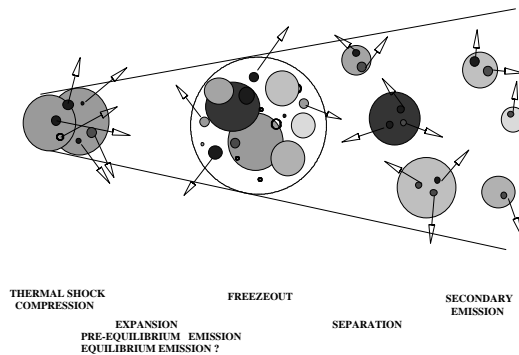PRE-EQUILIBRIUM EMISSION
EQUILIBRIUM EMISSION ?

Fig. 1. Schematic picture of collision leading to expansion and multifragmentation.

Figure 1 presents a schematic picture in which central collision of two heavy nuclei leads to multifragmentation. The collision produces a thermal shock and some compression. Reacting to this, the nucleus expands to low density, clusters and disassembles. This disassembly stage is labelled "freeze-out" in the figure. In an ideal situation this disassembly would be that of a thermally and chemically equilibrated nucleus. In practice this ideal state may not be reached and the final product distribution may include fragments and particles originating from non-equilibrium processes and reflecting correlations already present in the separated projectile and target nuclei [1,2]. Distinguishing between these different production mechanisms of fragment and light particle production is difficult but essential to our understanding of the multifragmentation process.

We are currently attempting to employ coalescence model analyses of light particle emission to probe the size of the emitting system in these collisions. The very similar formal structures of such models applied in both non-equilibrium and equilibrium conditions [3–5] suggest that they can provide a natural framework for this purpose. Under suitable conditions extraction of coalescence radii provides size information the analogous to

that obtained in particle–particle correlation measurements [6,7]. The main prediction of coalescence models is the existence of a power law relationship between complex clusters and nucleons [5]. The cross section for emission of a light cluster of mass number A, containing Z protons and N neutrons is related to the cross section for emission of protons and neutrons at the same momentum per nucleon. In practice the equation is often modified to take into account the fact that neutron cross sections are usually not measured in experiments, therefore an assumption is made that the neutron and proton momentum distributions are the same (except for a Coulomb shift) and their relative yields are given by the isospin of the combined system. The equation then becomes:

$$\frac{d^3 N_A}{dp^3} = R_{np}^N \frac{1}{N! Z!} \left(\frac{2s+1}{2^A} \right) \left(\frac{4\pi}{3} P_0^3 \right)^{A-1} \left(\frac{d^3 N_p}{dp^3} \right)^A , \qquad (1)$$

where P_0 represents the radius in the momentum space, and s is the cluster spin. The factor R_{np} is the ratio of neutron and proton numbers, usually taken to be those in the composite system formed from the projectile and target nuclei; *i.e.*, $R_{np} = (N_t + N_p)/(Z_t + Z_p)$.

Although originally created for high and relativistic energy collisions, the coalescence model has been applied to reactions over a wide range of energies, even to reactions with beam energy as low as $9A$ MeV [8]. At lower beam energies, however, certain problems emerge. The most important one, which cannot be neglected, is the Coulomb repulsion between the source and the outgoing particle. To account for this Awes *et al.* [9] presented a Coulomb corrected coalescence model. In the laboratory frame their derived relationship between the differential cross section of the observed cluster and that of the proton is:

$$\frac{d^2 N(Z,N,E_A)}{dE_A d\Omega} = R_{np}^N \frac{A^{-1}}{N! Z!} \left(\frac{\frac{4}{3}\pi P_0^3}{[2m^3(E-E_c)]^{\frac{1}{2}}} \right)^{A-1} \left(\frac{d^2 N(1,0,E)}{dE d\Omega} \right)^A , (2)$$

R_{np}, A, Z, N are the same as in Eq. (1), E_c is the Coulomb repulsion per charge unit between the source and outgoing particle and m is the nucleon mass. The double differential multiplicities $d^2 N(Z,N,E_A)/dE_A d\Omega$ and $d^2 N(1,0,E)/dE d\Omega$ for a cluster A and protons, respectively, should be taken at the energies corresponding to the same surface velocity; *i.e.*, the velocity before Coulomb acceleration. Thus $E_A = AE - NE_c$.

Various formulations of the coalescence model have been proposed to establish the relationship between the coalescence parameter P_0 and the size of the interaction volume. Sato and Yazaki [3] have presented a solution to this problem in the frame work of the density matrix formalism. An

important feature of this approach is that thermal and chemical equilibrium are not required. Sato and Yazaki showed that the coalescence volume is related to the internal wave function of the composite particle and the spatial distribution of the constituent particles in the emission region.

$$\frac{d^3 N_A}{d^3 P_A} = R_{np}^N A^{\frac{5}{2}} \frac{2s+1}{2^A} \left(\frac{\hbar}{m_0}\right)^{A-1} \left((1+\beta_T \nu_A)\frac{4\pi\nu_A\nu}{\nu_A+\nu}\right)^{\frac{3}{2}(A-1)} \left(\frac{d^3 N_p}{d^3 P}\right)^A.$$
(3)

Here ν and ν_A, respectively, characterize the spatial extent of the emitter and emitted cluster wave functions (assumed to be Gaussian), s is the spin of the cluster and R_{np} is the neutron to proton ratio of the coalescence source. While this model does not assume thermal or chemical equilibrium it does contain a temperature-like parameter,

$$\beta_T = \frac{\hbar^2}{2m_0 T}$$
(4)

which characterizes the momentum distribution of the contributing particles at the time of emission. The numerical values of ν_A are 0.20 fm^{-2} for deuterons, 0.36 fm^{-2} for tritons and ^{3}He and 0.58 fm^{-2} for alpha particles [3]. The equivalent sharp radius of the source is given by $R = \sqrt{5/2\nu}$.

The thermal coalescence model was introduced by Mekjian [4]. His model assumes that chemical equilibrium has been reached and the particles are emitted at the freeze-out density where the interactions stop. The momentum radius, P_0, can then be related to the volume of the thermal system at the freeze-out density in the following way:

$$V = \left(\left(\frac{Z!N!A^3}{2^A}\right)(2s+1)e^{(E_0/T)}\right)^{1/(A-1)} \frac{3h^3}{4\pi P_0^3},$$
(5)

where Z, N and A are the same as in Eqs (1) and (2), E_0 is the cluster binding energy and s the spin of the emitted cluster and T is the temperature of the system. If the source is assumed to be spherical its radius is given by

$$R = \left(\frac{3V}{4\pi}\right)^{(1/3)}.$$

For very high temperatures the factor $e^{E_0/T}$ is approximately equal to 1 and the relation between P_0 and V corresponds simply to what is expected from the phase space density. It should be noted that in this equilibrium model the cluster yields are related to observed nucleon yields, in contrast to non-equilibrium coalescence models where they are related to primary nucleon yields.

2. Molecular dynamics and system evolution

To explore the utility of the coalescence model to follow the evolution of a nuclear-like system, we have turned to classical molecular dynamics simulations. Such simulations allow us to elucidate the relationship between cluster yields and the properties of the emitting system in a straight-forward fashion. CMD is exact at a classical level; *i.e.*, it contains all the correlations necessary to build finite systems and, at sufficiently high excitation energy, to follow their disassembly. Thus if we follow the dynamics for a long period of time we can obtain final fragment distributions and all of the properties of interest for the final fragments; *i.e.*, their kinetic energies, mass and charge numbers, *etc.* From the mass distributions we can calculate the corresponding P_0 and deduce the apparent size of the disassembling system. Most importantly we can test the basic ingredients of the models, such as the possible occurrence of chemical equilibrium, as assumed in thermal coalescence models [4].

The CMD model of Latora *et al.* [10] was used to simulate disassembly in the absence of a Coulomb field. In that model the spinless particles interact through Yukawa two-body potentials. The potential between two identical particles is purely repulsive while for non-identical particles the potential is repulsive at short range and attractive at long range. The ground state "nuclei" have a deuteron-like cluster structure. This is of course very different from real finite nuclei where, at most, some alpha structure can be found. Also the deuterons have ~ 11 MeV binding energy. In the ground state the system is a solid. More details are given in [10–12].

To perform a calculation we initially prepared the nucleus in its ground state (a solid) and give to its particles some momenta corresponding to a Maxwell Boltzmann distribution at temperature T. In this way we know the initial source radius and excitation energy. Because of this initial T (or excitation energy E^*) the system will expand and if T is high enough, it will undergo fragmentation. The evolution is followed for a long time (1000–2000 fm/c), and the distribution of final fragments, which are then well separated, are constructed. We stress that all the formulas employed for the coalescence model are perfectly valid for this classical system apart from some obvious modifications such as setting the spins of the particles equal to zero. All P_0 values presented were calculated using observed final nucleon yields.

In these classical systems the excitation energy per nucleon is proportional to $(3/2)T$, while in the nuclear system it is initially proportional to T^2/K where K is in the range of 8–15. As a result, at a particular temperature, the excitation energy per nucleon in the classical system is significantly

higher than that of the nuclear system. In the classical system this 5 MeV temperature is above the critical temperature and the expansion is fairly explosive [10–12].
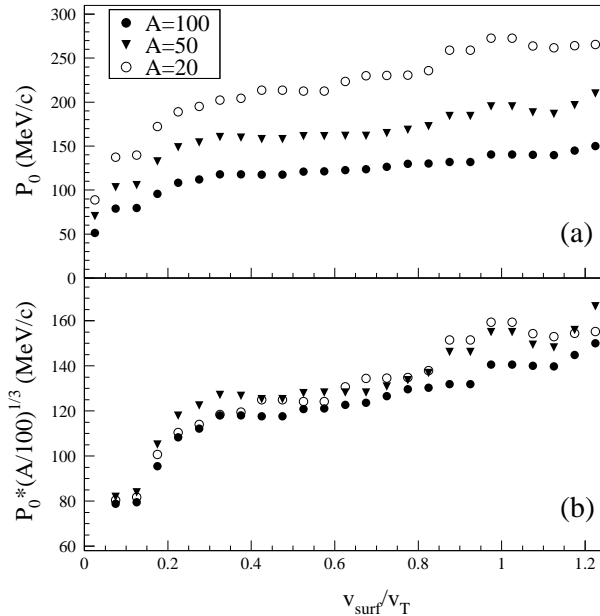

Fig. 2. (a) P_0 vs deuteron velocity (in units of a thermal velocity) and (b) P_0 scaled with the source masses both at $T = 5$ MeV. Results are presented for $A = 20$, 50 and 100.

In figure 2(a) we show P_0 vs. velocity (in units of a thermal velocity $v_T = \sqrt{4T/m}$), and in figure 2(b) the same data scaled by the total mass (divided by 100) to the 1/3 power. P_0 decreases as the mass increases. The scaling with the cube root of A is quite good and clearly demonstrates that P_0 gives direct information about the size of the system. This result follows directly from the Law of Mass Action [4].

It is clear from figure 2 that the value of P_0 depends on the particle velocity v, and is smaller at lower v. This indicates that, at the time when the less energetic particles are emitted, the system has expanded. Therefore different velocities correspond to different source sizes and times of emission. To explore further the relation between time of emission and velocity of the particle we have repeated the $T = 5$ MeV calculation, stopping the calculation at 100 fm/c.

In figure 3(a) the calculated values of P_0 obtained from deuteron yields at 100 fm/c (open squares) are compared with those determined from the earlier calculation which extended to 1000 fm/c (full circles). Notice that the
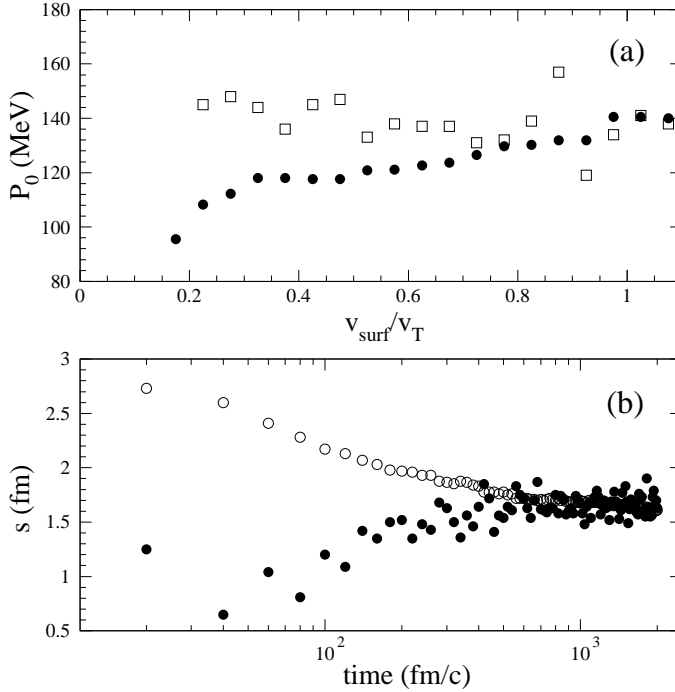
Fig. 3. (a) P_0 for deuterons at $T = 5$ MeV calculated at two different expansion times 100 fm/c (open squares) and 1000 fm/c (full circles). (b) Average nucleon separation in nascent deuterons as a function of time. $E_d < 30$ MeV (open circles), $E_d > 30$ MeV (full circles).

P_0 values derived from the particles emitted in the very early stages of the reaction are constant (within statistical fluctuations). Also, for high v, P_0 is independent of the time when the calculations are stopped. This confirms that the most energetic particles dominate the early emission. Thus these particles can be used to probe the early stages of the dynamics.

Within the model we can also study the location of the particles in r-space before they are emitted. This gives us useful information regarding the possible establishment of thermal and/or chemical equilibrium. In figure 3(b) we plot, as a function of time, the average relative separation distances between protons and neutrons which eventually coalesce into a deuteron. the results are displayed for deuterons having kinetic energies less than 30 MeV (open circles) and those with energies larger than 30 MeV (full circles). Since the initial temperature is 5 MeV particles having energies larger than 30 MeV are quite energetic.

In the figure we see that those very energetic particles have to be initially quite close in r-space in order to form a deuteron. In fact, on average their starting distance is less than 1 fm, which is smaller than the deuteron radius of about 1.5 fm. If two energetic particles are close both in r and p-space, they coalesce and form the deuteron. On the other hand, lower energy deuterons are made of nucleons that can be located quite far apart in r-space at time $t = 0$. These nucleons wander inside the system and it is only at larger time that they find each other to form the deuteron. From this result it is quite clear that a statistical model seems unjustified for particles of high energy but might be applicable for emission of lower energy particles. Within the CMD approach the possibility of chemical equilibrium as assumed by reference [4] becomes more probable for the less energetic particles.

Finally in figure 4, we plot radii derived from P_0 for $A=100$ at various temperatures. Notice the large difference between the Sato–Yazaki and Mekjian model results. In addition to reflecting the cluster size cor-
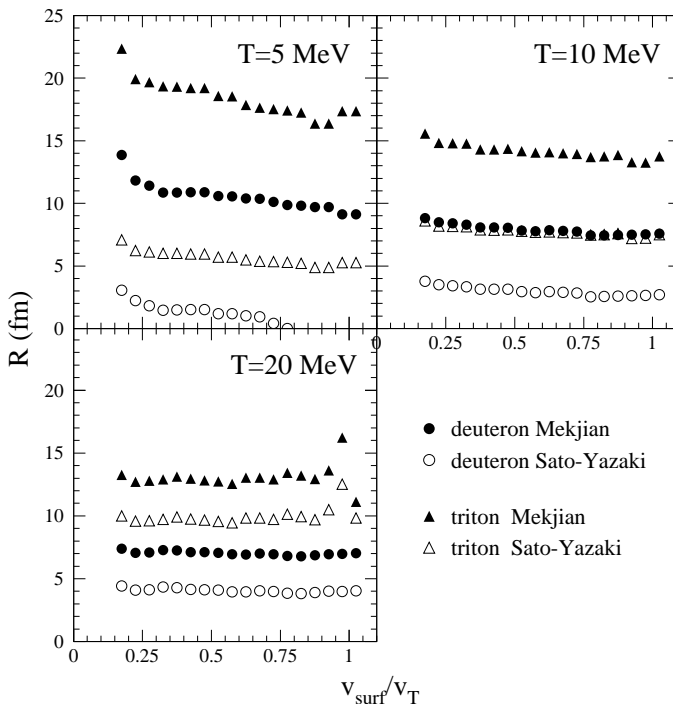

Fig. 4. Calculated radii for d and t clusters at $T = 5$, 10 and 20 MeV. Circles are for d clusters and triangles for t clusters. Full symbols for Mekjian model; open symbols for Sato–Yazaki model.

rection contained in the Sato–Yazaki density matrix model, this difference arises from the different temperature dependencies in the two models. More specifically it arises from the $e^{-BE/T}$ term in the thermal model approach, all the other terms being equivalent in the two formalisms. Since in CMD the clusters are quite strongly bound as compared to real nuclei, the BE term becomes very important, resulting in the large discrepancy at small T. The two approaches give closer results at high T where the BE term can be neglected. The very large values derived from the thermal model at low T argue against the assumption of chemical equilibrium for the particular cases considered, which as we have already noted, are quite explosive.

3. Application to intermediate energy nuclear collisions

To make a quantitative evaluation of the utility of coalescence model techniques in following the dynamics of expanding systems we recently used the combined TAMU CsI Ball-Neutron Ball detection system to detect light charged particles, fragments and neutrons emitted in the reactions of ^{12}C + ^{116}Sn, ^{22}Ne + Ag, ^{40}Ar + ^{100}Mo and ^{64}Zn + ^{89}Y, all at 47A MeV projectile energy [13, 14]. In QMD transport model calculations with the code, CHIMERA [15], the particular set of target and projectile combinations used in our experiment are predicted to lead, after pre-equilibrium emission of particles, to excited composite nuclei of very similar mass but having excitation energies and degrees of expansion which increase with increasing projectile mass. Violent events corresponding to the 10% of the reaction cross section having the highest charged particle and neutron multiplicities were selected for detailed coalescence model analyses. For such events multifragment emission was observed to become increasingly more probable as the projectile mass increases. Greater detail on these measurements is provided in Refs [13] and [14].

3.1. Correlation between kinetic energy and time

We have carried out analyses of nucleon and light cluster emission as a function of particle velocity, basing our approach on coalescence model techniques [3–5,9]. The possible application of the coalescence approach as a function of ejectile velocity to follow the dynamics of an expanding system is already suggested by the discussion of the classical molecular dynamics calculations for expanding systems, presented in the previous section and is reinforced by results of simulations carried out with the QMD model code, CHIMERA [15] (see figure 5). In the calculations for 47A MeV projectiles, the first light particles are emitted at $\sim$50 fm/c after contact. These and subsequent pre-equilibrium particles remove significant amounts of both mass and energy from the expanding composite nuclei. For each reaction
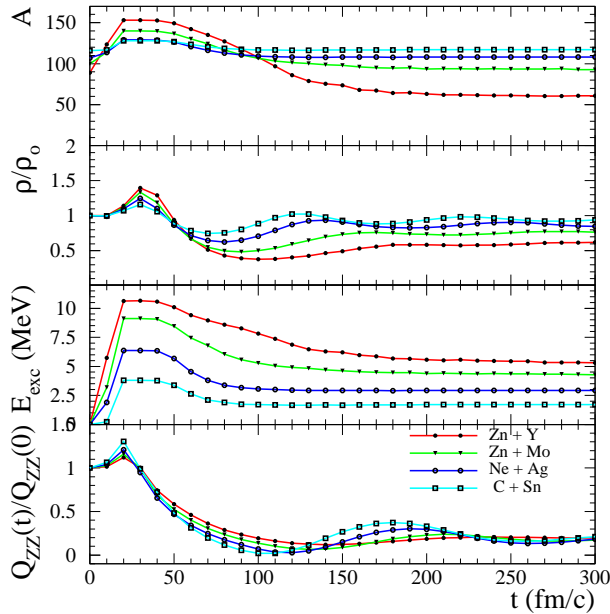
Fig. 5. CHIMERA QMD model calculations of the time evolution of the properties of the largest identifiable fragments produced in reactions induced by 47A MeV projectiles. From top to bottom: The mass number, the normalized density, the excitation energy per nucleon and the normalized second moment of the momentum distribution, a measure of the degree of thermal equilibration. The calculations are for an impact parameter range of 0–3 fermis.

the hot composite reaches its minimum average density close to 100 fm/c. At that point thermal equilibrium appears to be established. Over the time span from first emission to thermalization there is a monotonic decrease of the average kinetic energies of the emitted particles. A strong correlation between energy and emission time has, in fact, been clearly demonstrated in reactions induced by ^{40}Ar projectile energies of 25 [16] and 34 MeV/u [17] where light particle correlation measurements were employed to determine the mean times for emission of hydrogen ejectiles as a function of particle velocity. Thus both theoretical models and experiments suggest that the relationship between emission time and ejectile kinetic energy may be exploited to follow the time evolution of the system.

3.2. Preliminary system characterization — emission sources

Invariant velocity plots of the light particle spectra show striking similarites indicating a common emission mechanism for the higher energy particles

and clusters for all four systems studied [13,14]. This is a strong signature for the dominance of dynamic (rather than statistical) emission of these higher kinetic energy particles.

A common technique to characterize light particle emission in this energy range has been to fit the observed spectra assuming contributions from three sources, a projectile-like (PLF) source, an intermediate velocity (NN) source and a target-like (TLF) source. Such a source fit was employed to estimate the multiplicities and energy emission at each stage of the reaction. We emphasize that the event selection is on the most violent and presumably more central collisions. In the fitting process, which assumes isotopic emission and a Maxwellian spectral shape in the particular source frame considered, accounting for forward emitted particles with projectile-like velocities requires the PLF source. We consider these particles to be of pre-equilibrium emission origin and not to be evaporated from a fragment. From the multiplicities of emitted species associated with each source the masses and excitation energies of the hot nuclei which remain after the early (PLF and NN) emission were determined. The mass numbers, obtained by subtracting the mass removed by projectile-source and intermediate source particles from the total entrance channel mass are ∼110. The excitation energies, determined using calorimetric techniques to evaluate the excitation of the TLF source, increased with projectile mass from 2.6 MeV/u for ^{12}C+ ^{116}Sn to 6.9 MeV/u for ^{64}Zn + ^{89}Y. While the source fits establish a qualitative or semi-quantitative picture of ejectile sources and system evolution following the time evolution of a continuously evolving system in more detail than has previously been attempted requires a more sophisticated approach.

3.3. Determination of the coalescence parameter, P_0

Because the goal was to derive information on the time evolution of the emitting system, our analysis was not limited to determining average P_0 values appropriate to the higher energy portions of the particle spectra, as is common in previous work. Instead, for d, t, ^{3}He and ^{4}He, P_0 was calculated as a function of V_{surf}, the velocity of the particle at the nuclear surface prior to Coulomb acceleration, using the Coulomb corrected coalescence model formalism of Awes *et al.* [9], Eq. (2).

To minimize contributions from secondary decays our analysis was performed using spectra from which the TLF contributions were removed by subtraction of the target-like-source yields obtained in the source fits from the observed experimental yields at angles where the PLF source is negligible. In this work P_0 was determined using the observed proton yields. This choice is at least consistent with the apparent successes of statistical models which assume the existence of equilibrium or near-equilibrium conditions in hot expanding nuclei [18–20].

3.4. N/Z ratios

In figure 6 (top), values of the observed $t/^3$He yield ratio are presented as a function of V_{surf}. These ratios are significantly higher than the N/Z ratios in the composite systems. We understand these to be the ratios of "free nucleons" [21] which participate in the coalescence. In Eqs (1)–(3), N_p, N_t, Z_p and Z_t enter the equation because measurements which include neutron information are relatively rare. It has typically been assumed, in most coalescence model analyses, that the neutron energy spectra are identical in shape to the Coulomb corrected proton spectra and that the neutron yields are simply N/Z times the proton yields, where N/Z is the neutron to proton ratio in the composite system. In this work, also, the neutron spectra are not measured. However, since within the framework of the coalescence model the yield ratios of two isotopes which differ by one neutron are essentially determined by the effective N/Z ratio in the coalescence volume. We have used values derived directly from the observed triton to ^{3}He yield ratio to determine the N/Z ratio used in this analysis. This use of
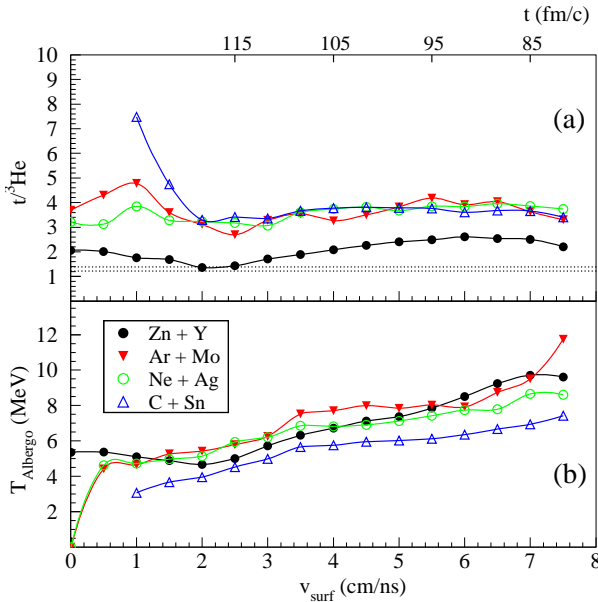

Fig. 6.   Experimental ratios of ^{3}H to ^{3}He emission yields (top) and double isotope yield ratio temperatures (bottom) as a function of Coulomb-corrected surface velocity. Data below ~ 4 cm/ns may have residual contributions from statistical evaporation. The horizontal bar in the top portion indicates the range of composite nucleus N/Z values for the systems studied. Time scales derived from CHIMERA QMD model calculations are indicated at the top of the figure.
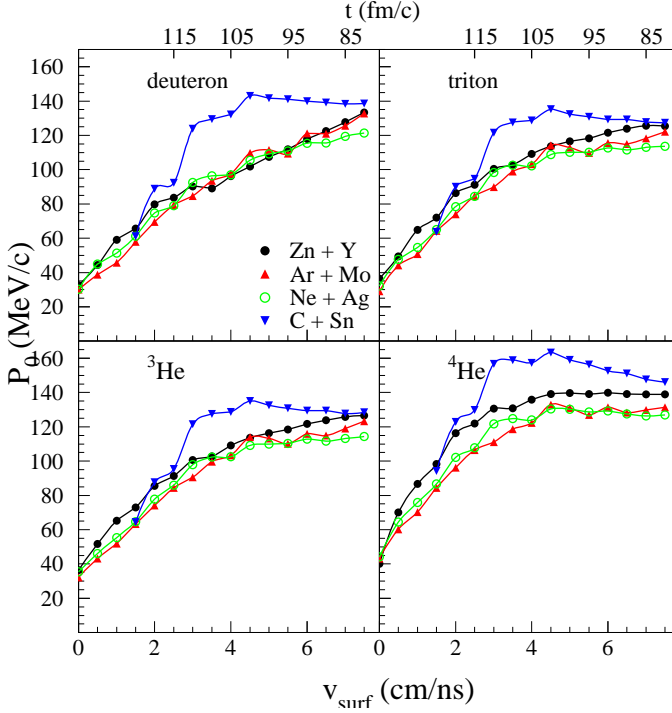
Fig. 7. Derived values of the coalescence parameter, P_0, as a function of surface velocity for p, d, t, ^{3}He and ^{4}He clusters emitted in the four reactions studied. The contributions of the ejectile spectra attributed to the TLF source have been subtracted from the experimental spectra at Lab = 38–52 degrees. PLF contributions are neglegible at that angle. Time scales derived from CHIMERA QMD model calculations are indicated at the top of the figure.

this "effective" N/Z ratio is a self-consistent approach but may mean that some actual differences in neutron and proton spectra are absorbed into this ratio [22, 23].

Figure 7 shows the results of an analysis of the resultant ejectile spectra (Experiment — TLF) for all four systems studied. As seen in figure 7, at high V_{surf} the four systems have similar limiting values of P_0 for a given cluster species, supporting the idea of a similar emission mechanism and a similar source size at the time of emission of the higher energy particles in the different reactions studied. The observed decreases of P_0 with decreasing surface velocity indicate changes in the emitting system.

The time scale presented at the top of Figs 6–9 is derived from the QMD model and indicates that a value of V_{surf} of 4 cm/ns is expected to sample the system near 105 fm/c. Below 4 cm/ns residual contributions from late stage

evaporative decay of the target-like source or secondary decay from light fragments [24], not removed by the fitting process, may still contribute.

3.5. Size evolution of the emitting system

For each model, deriving the size of the system from P_0 also requires knowledge of the temperature. To characterize the temperature at a particular emission time we have employed double isotope yield ratios. For a system at chemical and thermal equilibrium at a suitably low density, Albergo *et al.* [21] have shown that the temperature of the emitting system can be derived directly from the first chance emission double isotope yield ratios of two adjacent isotopes of two different elements. In a more recent work by Kolomiets *et al.* [25], essentially the same result is derived when only thermal equilibrium is assumed. If the particle energies are well correlated with emission time, and secondary emission contributions contribute primarily at the lower energies, derivations of double isotope yield ratio temperatures as a function of particle energy may be relatively uncontaminated by secondary emission processes, except at the lower energies. On the other hand, it should be clearly noted the apparent temperature derived for the earliest stage, while indicative of the particle momentum distribution at that emission time, is not the temperature since the dynamic transport calculations indicate that the condition of thermal equilibrium is established only after some particle emission occurs. Note that the Mekjian model and the model proposed by Albergo *et al.* to derive double isotope ratio temperatures [21] are, in fact, equivalent and the assumed validity of this model incorporating chemical equilibrium is implicit in all recent works which use double isotope yield ratios to determine temperatures [26–28].

3.6. Temperature

We have derived the double isotope yield ratio temperature, $T_{\mathrm{H\,He}}$, as a function of, V_{surf} from the yields of d, t, ^{3}He and ^{4}He particles, again corrected by subtracting the contributions associated with the TLF. The derived temperatures, presented as a function of V_{surf} in the bottom of figure 6, increase slowly with projectile mass and decrease with decreasing V_{surf}.

The QMD calculations suggest that the system equilibrates rapidly but global thermal equilibrium is not completely established when the first particles are emitted. Thus the temperatures at high V_{surf} should be considered only as approximations.At the lowest values of V_{surf}, values of $T_{\mathrm{H\,He}}$ in the 4–5 MeV range, similar to those spectral integrated values seen at comparable excited energies in other experiments [26–28] are observed. Indeed the $T_{\mathrm{H\,He}}$ values observed in this lower energy region are very similar to those

calculated using the sequential evaporation code GEMINI [29]. Since spectra at these lower velocities may still contain a contribution from late stage evaporation we do not attempt to extract emission system sizes for $V_{surf} <$ 4 cm/ns.

3.7. System sizes

To extract nuclear size information from the P_0 and T determinations, both the density matrix formalism of Sato and Yazaki [3] and the thermal model formalism of Mekjian [4] were employed. For this evaluation the temperature characterizing the emission spectrum was set equal to the instantaneous Albergo temperature at the corresponding surface velocity.
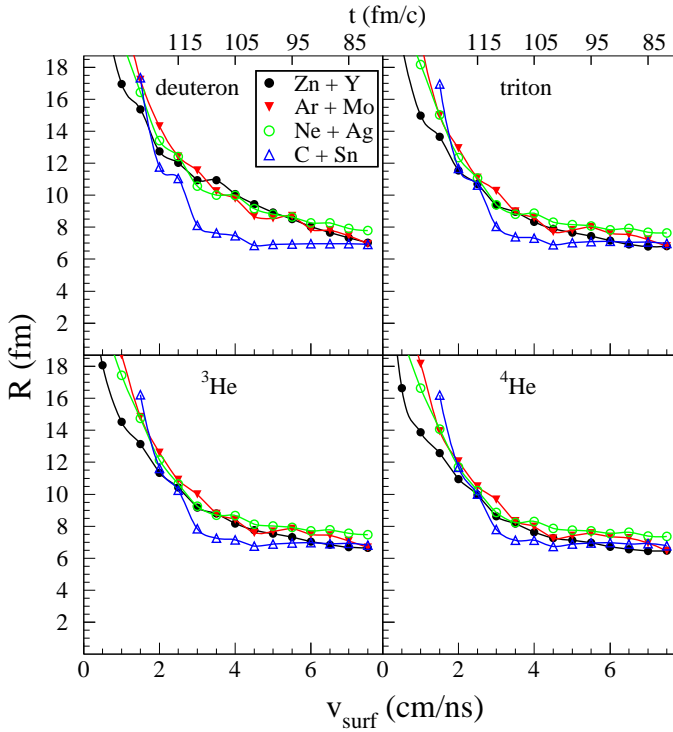

Fig. 8. Equivalent sharp radii derived from the Mekjian model. Radii for assumed spherical sources are presented as a function of surface velocity for d, t, ^{3}He and ^{4}He clusters. The values of P_0 employed are those of figure 7. Time scales derived from CHIMERA QMD model calculations are indicated at the top of the figure.

For both models, we present in figures 8 and 9, equivalent sharp cut-off radii for assumed spherical sources as derived from the P_0 values presented in figure 7. For each model, the sizes derived from the highest velocity

particles show little dependence on projectile type and only for the lower
energy ejectiles is a difference seen. The absolute values of the radii are
larger for deuterons and smaller for alpha particles, possibly reflecting the
very different binding and spatial extent of these clusters [3]. Such differences
have been indicated in previous coalescence model studies [3–5, 9]. That
the differences persist in the density matrix model which attempts to take
the cluster size into account is interesting and, if it does not result from
simplifying assumptions implicit in the model, may imply some different
freeze-out densities required for survival of different cluster species.
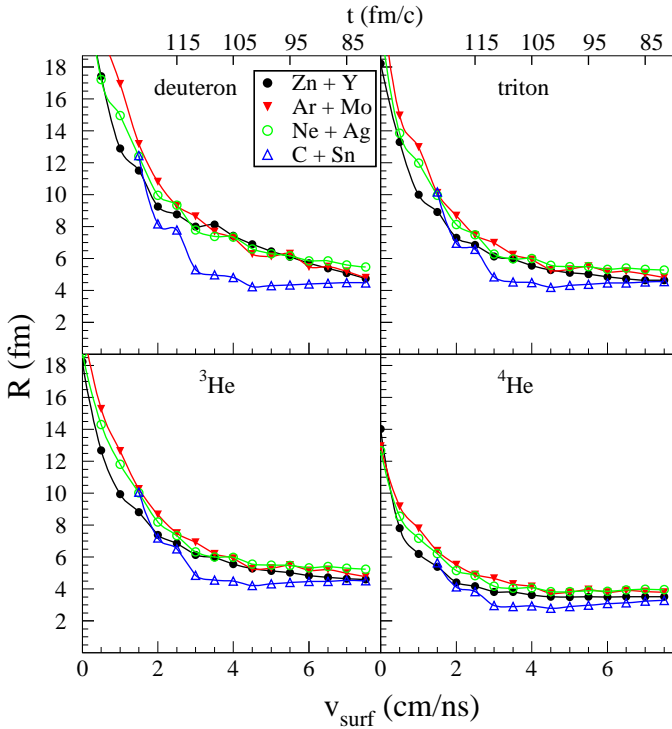

Fig. 9. Equivalent sharp radii derived from the Sato–Yazaki model. Radii for
assumed spherical sources are presented as a function of surface velocity for d, t,
^{3}He and ^{4}He clusters. The values of P_0 employed are those of figure 7. Time scales
derived from CHIMERA QMD model calculations are indicated at the top of the
figure.

The size parameters are clearly different, reflecting differences in the
models. The S–Y model equivalent sharp radii are smaller than the radii of
normal density nuclei in this mass range. This is true even if no correction is
made for cluster size and apparently reflects the particular analytical formu-

lation of the Sato–Yazaki model [3]. The values of thermal model equivalent sharp radii at the highest values of V_{surf} are slightly larger than those expected for the composite nuclei at normal density. At $V_{\text{surf}} = 7$ cm/ns they correspond approximately to $R = 1.3 A^{(1/3)}$ where A is the total entrance channel mass.

For ^{12}C induced reactions the derived radii for the different particles indicate very little change of size during the particle emission phase. Progressively larger increases of the radii during particle emission are indicated for reactions with the heavier projectiles. While the absolute values of the derived radii are different for the two models, for a given ejectile, the ratio $R(V_{\text{surf}} = 4 \text{ cm/ns})/R(V_{\text{surf}} = 7 \text{ cm/ns})$, a measure of the relative radius increase, is found to increase with projectile mass in a very similar fashion in the two models. Since the derived absolute radii can be subject to systematic uncertainties both in the measurements and in the model assumptions, we choose to derive densities at freeze-out from the relative changes averaged over the four particles.

3.8. Densities

To determine the average density associated with the system when $V_{\text{surf}} = 4$ cm/ns. We first assumed that the highest velocity particles are emitted from an object of mass equal to the sum of the masses of the target and projectile nuclei and of density equal to 0.90 P_0 (see figure 5). We then used the relative values of the radii derived from the t, ^{3}He and ^{4}He data at 4 and 7 cm/ns and took the mass of the primary emitter at $V_{\text{surf}} = 4$cm/ns to be the mass remaining in the target-like source. From the thermal model we find that the average densities sampled at $V_{\text{surf}} = 4$ cm/ns are 0.81 ρ_0, 0.54 ρ_0, 0.45 ρ_0 and 0.36 ρ_0 for the ^{12}C, ^{22}Ne, ^{40}Ar and ^{64}Zn induced reactions, respectively, with uncertainties of $\pm 20\%$ of these values. The corresponding values obtained using the Sato–Yazaki model are 0.94 ρ_0, 0.58 ρ_0, 0.45 ρ_0 and 0.38 ρ_0.

Our energy-density results presented in figure 10 are in very reasonable agreement with results of the CHIMERA QMD calculation when an equation of state with $K = 200$ MeV is employed. For this soft equation of state the calculations indicate entry into the spinodal region to the left of the dashed line, $V_s^2 = 0$. A harder equation-of-state with $K = 380$ MeV results in less expansion and poorer agreement with the experimental results.
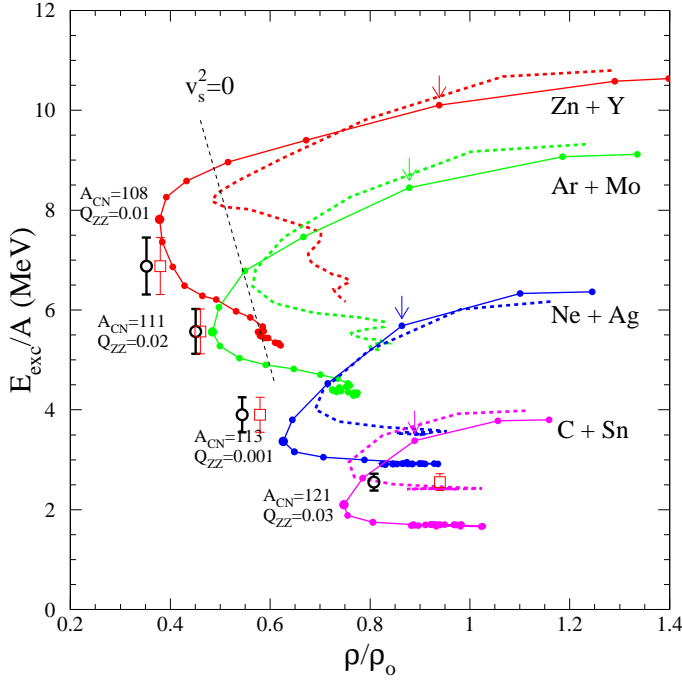
Fig. 10. Excitation energy-density values at freeze-out. The symbols represent the excitation energy-density values (open circles — Mekjian model, open squares — Sato–Yazaki model) derived from coalescence model analyses of the light cluster emission. They are compared to CHIMERA QMD model trajectories in the excitation energy per nucleon-normalized density plane calculated for central collisions in the four different systems studied. Calculations for a soft, $K = 200$ MeV, equation-of-state are represented by solid lines. Calculations for a hard, $K = 380$ MeV, equation-of-state are represented by thick dashed lines. The trajectories start at the time of maximum density. The small dots mark time increments of 10 fm/c. Arrows indicate the time of first emission of particles (near 50 fm/c after contact). Both times and Q_{zz} values are indicated at the minimum calculated densities (large solid dots). To the left of the dashed line, $V_s^2 = 0$, is the spinodal region.

3.9. Caloric curve

We present in figure 11 the double isotope yield ratio temperatures at 4.0 cm/ns plotted against excitation energy. The results indicate a nearly flat caloric curve with $T \sim 7$ MeV at excitation energies from 3.5 to 7 MeV per nucleon. At the higher excitation energies, the double isotope yield ratio temperatures near 7 MeV indicated for the expanded low density systems isolated here are consistent with the limit suggested in our earlier work on

the caloric curve for $A \sim 125$ nuclei in which we found a temperature of 6.8 ± 0.5 MeV at 4.3 MeV/u excitation energy [30]. The general shape of the caloric curve in figure 11 can then be understood as reflecting first, at lower excitations, primarily the washing out of shell effects and collectivity [31,32] and later, at higher energies, the expansion of the system.
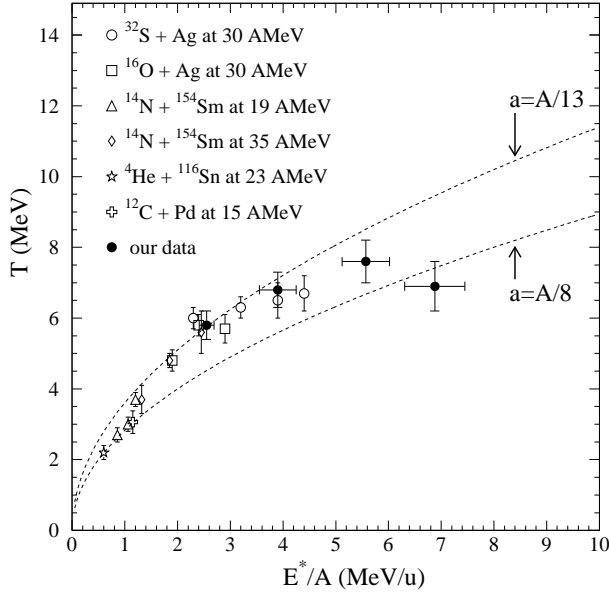

Fig. 11. Caloric curve for nuclei with $A \sim 110$. Double isotope yield ratio temperatures derived in the present work are combined with results reported previously by Wada *et al.* obtained with a different technique [30]. Dashed lines indicate trends of a Fermi gas model calculation with two different choices of level density parameter.

4. Summary and conclusions

The work discussed here indicates that coalescence model studies of light cluster emission can indeed be used in the intermediate energy regime to follow the dynamic evolution of excited systems. Information on the space-time evolution of the system complementary to that contained in HBT measurements [6,7] can be obtained in a relatively simple manner.

Both classical and quantum molecular dynamics calculations lead to caloric curves similar to that observed here [33,34]. If a temperature limit of thermally equilibrated nuclei is reached, these calculations suggest that the system clusters and the nucleons with high kinetic energies stream out

of the expanding system, creating a natural limit to the momentum distribution and to the excitation energy of the remaining nucleus over a wide transitional region. This is also suggested by the saturation of the Lyapunov exponent in CMD studies [10]. The evolution of the volume of the system is very important in determining the caloric curve [33–35]. Observed differences in caloric curves extracted from different reaction systems may reflect the particular dynamic evolution of the system being studied and great care must be taken to understand this dynamics.

REFERENCES

[1] P.B. Grossiaux, J. Aichelin, *Phys. Rev.* **C56**, 2109 (1997).

[2] E. Colin *et al.*, *Phys. Rev.* **C57**, R1032 (1998).

[3] H. Sato, K. Yazaki, *Phys. Lett.* **B98**, 153 (1981).

[4] A.Z. Mekjian, *Phys. Rev.* **C17**, 1051 (1978); *Phys. Rev. Lett.* **38**, 640 (1977); *Phys. Lett.* **B89**, 177 (1980).

[5] L.P. Csernai, J.I. Kapusta, *Phys. Rep.* **131**, 223 (1986).

[6] W. Bauer *et al.*, *Ann. Rev. Nucl. and Part. Sci.* **42**, 77 (1992).

[7] D. Ardouin, *Int. J. Mod. Phys.* **E6**, 391 (1997).

[8] T.C. Awes *et al.*, *Phys. Rev.* **C25**, 2361 (1982).

[9] T.C. Awes *et al.*, *Phys. Rev.* **C24**, 89 (1981).

[10] V. Latora, *et al.*, *Phys. Rev. Lett.* **73** 1765 (1994); P. Finocchiaro, *et al.*, *Nucl. Phys.* **A600**, 236 (1996); A. Bonasera, *et al.*, *Phys. Rev. Lett.* **75**, 3434 (1995); A. Bonasera, *Phys. World* **12**, 20 (1999).

[11] C.O. Dorso *et al.*, *Phys. Rev.* **C60**, 34606 (1999).

[12] R.J. Lenk *et al.*, *Phys. Rev.* **C42**, 372 (1990).

[13] J. Cibor *et al.*, *Phys. Lett.* **B473**, 29 (2000).

[14] K. Hagel *et al.*, submitted to *Phys. Rev.* **C**, (March 2000).

[15] J. Lukasik, Z. Majka, *Acta Phys. Pol.* **B24**, 1959 (1993).

[16] Z.Y. He *et al.*, *Phys. Rev.* **C57**, 1824 (1998).

[17] C.J. Gelderloos *et al.*, *Phys. Rev.* **C52**, R2834 (1995).

[18] D.H.E. Gross *Phys. Rep.* **279**, 119 (1997).

[19] J. Bondorf *et al.*, *Nucl. Phys.* **A433**, 321 (1985).

[20] W.A. Friedman, *Phys. Rev.* **C42**, 667 (1990).

[21] S. Albergo *et al.*, *Nuovo Cimento* **A89**, 1 (1985).

[22] A. Bonasera, G.F. Bertsch, *Phys. Lett.* **B195**, 521 (1987).

[23] J. Cibor *et al.*, to be published in *Isospin Physics in Heavy Ion Collisions at Intermediate Energies*, Nova Science Publishers, eds B.-A. Li and W.O. Schroeder.

[24] N. Marie and the INDRA Collaboration, *Phys. Rev.* **C58**, 256 (1998).

[25] A. Kolomiets *et al.*, *Phys. Rev.* **C55**, 1376 (1997).

[26] J. Pochodzalla *et al.*, *Phys. Rev. Lett.* **75**, 1040 (1995).

[27] J.A. Hauger *et al.*, (EOS Collaboration), *Phys. Rev.* **C57**, 764 (1998).

[28] Y.G. Ma *et al.*, *Phys. Lett.* **B390**, 41 (1997).

[29] R.J. Charity *et al.*, *Nucl. Phys.* **A483**, 371 (1988).

[30] R. Wada *et al.*, *Phys. Rev.* **C39**, 497 (1989).

[31] S. Shlomo, J.B. Natowitz, *Phys. Rev.* **C44**, 2878 (1991).

[32] J.N. De *et al.*, *Phys. Rev.* **C57**, 1398 (1998).

[33] A. Strachan, C.O. Dorso, *Phys. Rev.* **C58**, R632 (1998); *Phys. Rev.* **C59**, 285 (1999).

[34] Y. Sugawa, H. Horiuchi, *Phys. Rev.* **C60**, 607 (1999).

[35] L.G. Moretto *et al.*, *Phys. Rev. Lett.* **76**, 2822 (1996).